New model for capturing the variations of fertilizer-induced emission factors of N_2O

Feng Zhou, Ziyin Shang, Zhenzhong Zeng, Shilong Piao, Philippe Ciais, Peter Raymond, Xuhui Wang, Rong Wang, Minpeng Chen, Changliang Yang, et al.

AGU PUBLICATIONS

Global Biogeochemical Cycles

RESEARCH ARTICLE
10.1002/2014GB005046

Key Points:
- Our models are powerful to perform upscaling of N_2O fluxes
- Climate dominates the EF distribution of China's agricultural soils
- China's averaged N_2O EF for paddy rice is twice as large as IPCC Tier 1 default

Supporting Information:
- Texts S1–S3, Figures S1–S9, and Tables S1–S3

Correspondence to:
F. Zhou,
zhouf@pku.edu.cn

Citation:
Zhou, F., et al. (2015), New model for capturing the variations of fertilizer-induced emission factors of N_2O, *Global Biogeochem. Cycles*, *29*, 885–897, doi:10.1002/2014GB005046.

Received 1 DEC 2014
Accepted 17 MAY 2015
Accepted article online 20 MAY 2015
Published online 29 JUN 2015

New model for capturing the variations of fertilizer-induced emission factors of N_2O

Feng Zhou[1], Ziyin Shang[1], Zhenzhong Zeng[1], Shilong Piao[1], Philippe Ciais[2], Peter A. Raymond[3], Xuhui Wang[1], Rong Wang[2], Minpeng Chen[4], Changliang Yang[5], Shu Tao[1], Yue Zhao[6], Qian Meng[7], Shuoshuo Gao[1], and Qi Mao[1]

[1]Sino-France Institute of Earth Systems Science, Laboratory for Earth Surface Processes, College of Urban and Environmental Sciences, Peking University, Beijing, China, [2]Laboratoire des Sciences du Climat et de l'Environnement, CEA CNRS UVSQ, Gif-sur-Yvette, France, [3]Yale School of Forestry and Environmental Studies, Yale University, New Haven, Connecticut, USA, [4]Institute of Environment and Sustainable Development in Agriculture, Chinese Academy of Agricultural Sciences, Beijing, China, [5]Research Institute of Engineering Technology, Yunnan University, Kunming, China, [6]Department of Water Environmental Planning, Chinese Academy for Environmental Planning, Beijing, China, [7]Department of Statistics, University of Connecticut, Storrs, Connecticut, USA

Abstract Accumulating evidence indicates that N_2O emission factors (EFs) vary with nitrogen additions and environmental variations. Yet the impact of the latter was often ignored by previous EF determinations. We developed piecewise statistical models (PMs) to explain how the N_2O EFs in agricultural soils depend upon various predictors such as climate, soil attributes, and agricultural management. The PMs are derived from a new Bayesian Recursive Regression Tree algorithm. The PMs were applied to the case of EFs from agricultural soils in China, a country where large EF spatial gradients prevail. The results indicate substantial improvements of the PMs compared with other EF determinations. First, PMs are able to reproduce a larger fraction of the variability of observed EFs for upland grain crops (84%, $n = 381$) and paddy rice (91%, $n = 161$) as well as the ratio of EFs to nitrogen application rates (73%, $n = 96$). The superior predictive accuracy of PMs is further confirmed by evaluating their predictions against independent EF measurements ($n = 285$) from outside China. Results show that the PMs calibrated using Chinese data can explain 75% of the variance. Hence, the PMs could be reliable for upscaling of N_2O EFs and fluxes for regions that have a phase space of predictors similar to China. Results from the validated models also suggest that climatic factors regulate the heterogeneity of EFs in China, explaining 69% and 85% of their variations for upland grain crops and paddy rice, respectively. The corresponding N_2O EFs in 2008 are $0.84 \pm 0.18\%$ (as N_2O-N emissions divided by the total N input) for upland grain crops and $0.65 \pm 0.14\%$ for paddy rice, the latter being twice as large as the Intergovernmental Panel on Climate Change Tier 1 defaults. Based upon these new estimates of EFs, we infer that only 22% of current arable land could achieve a potential reduction of N_2O emission of 50%.

1. Introduction

Reactive nitrogen (Nr) entering agricultural soils from fertilizer applications worldwide results into a 43%–56% of global anthropogenic N_2O emissions [*Emission Database for Global Atmospheric Research*, 2014; *Saikawa et al.*, 2014]. This contribution is likely to increase in countries with intensive agricultural systems [e.g., China; *Zhou et al.*, 2014]. The nitrogen application rate (N) is an effective estimator of N_2O emissions and has been used to construct most national reports based on a fertilizer-induced emission factor (EF) approach [*Intergovernmental Panel on Climate Change* (*IPCC*), 2006]. According to IPCC methodology, the EF is calculated as the difference between N_2O emissions at an application rate and a control experiment with zero N divided by N. The EFs in IPCC Tier 1 are 1% for upland grain crops and 0.3% for paddy rice [*IPCC*, 2006].

These EF values of 1% and 0.3% are assumed to remain constant. However, considerable evidence from field experiments and meta-analysis demonstrates that EFs differ largely from the IPCC defaults and change with nitrogen additions, cultivation practice, and environmental conditions [*McSwiney and Robertson*, 2005; *Grace et al.*, 2011; *Hoben et al.*, 2011; *Kim et al.*, 2013; *Decock*, 2014; *Shcherbak et al.*, 2014; *Zhou et al.*, 2014] (see supporting information Figure S1). For example, *Shcherbak et al.* [2014], using 233 observations from 84 sites with at least three N input levels, found that EFs were higher when $pH < 7$ and that the percent change in EFs per unit of incremental N application rate (ΔEF) was systematically larger for legume crops,

Table 1. Comparisons Between Estimates of N_2O Emissions From PMs (This Study) and Previous Studies

		Performance in Upland			Performance in Rice			EF, (%)		E, (Gg N_2O-N/yr)[a]		
Source	Algorithm	R^2	BIC	RMSE	R^2	BIC	RMSE	Upland	Rice	Upland	Rice	Total
IPCC [2006]	Constant	--	−138	0.83	--	−149	0.62	1 ± 0.56	0.3 ± 0.35	328.5	23.6	352.1
Gao et al. [2011]	Constant	--	−126	0.84	--	−165	0.59	1.05 ± 0.02	0.41 ± 0.04	--	--	312.0
Wang et al. [2011b]	Constant	0.52	--	--	--	--	--	0.55 + 0.05	--	180.7	--	--
Lu et al. [2006][b]	Constant	0.35	−137	0.82	0.09	−145	0.59	0.69 ± 0.11	0.41 ± 0.09	226.7	32.3	258.9
Zou et al. [2009]	Constant	--	--	--	0.29–0.56	--	--	--	0.42 ± 0.06	--	33.1	--
Zhou et al. [2014]	Regional	--	−223	0.57	--	−230	0.48	1.11 ± 0.4	0.62 ± 0.3	365.0	49.2	414.2
Stehfest and Bouwman [2006]	RML	--	--	--	--	--	--	0.91 ± 0.42[c]		--	--	342.7
Akiyama et al. [2005]	RML	--	--	--	0.28	--	--	--	0.43 ± 0.1	--	33.9	--
Shcherbak et al. [2014][d]	SLF	0.02	300	1.4	0.04	−73	0.34	1.14	0.16	373.9	12.9	386.8
Shcherbak et al. [2014][e]	SLF	0.32	−136	0.82	0.10	−152	0.57	0.65 ± 0.18	0.56 ± 0.19	214.4	43.9	258.3
Chipman et al. [2002]	PMs	0.70	608	0.44	0.83	263	0.24	0.72 ± 0.22	0.57 ± 0.15	236.5	44.9	281.4
This study	PMs	0.84	-583	0.32	0.91	−381	0.17	0.84 ± 0.18	0.65 ± 0.14	272.6	51.2	323.8

[a] E for all EFs determinations are recalculated using our county-based N application rate in 2008.
[b] EF models are calibrated following methodology of *Lu et al.* [2006] but based on our N_2O observations.
[c] The data are for agricultural soils but never made a distinction between upland and rice.
[d] EF models are extracted from Table S3 in *Shcherbak et al.* [2014].
[e] EF models are calibrated following methodology of *Shcherbak et al.* [2014] but based our N_2O observations without two outliers from *Mei et al.* [2011].

for the case of ammonium nitrate applications, and for soils with organic carbon (SOC) >1.5%. A growing number of field observations have also examined the effects of temperature or moisture on N_2O fluxes at specific sites [*Schindlbacher et al.*, 2004; *Singurindy et al.*, 2009; *Troy and Tang*, 2011; *Dijkstra et al.*, 2012]. Yet the mechanism of how environmental factors (x_k) regulate the heterogeneity of EFs in agricultural soils remains elusive at regional or global scales [*Xu et al.*, 2012; *Butterbach-Bahl et al.*, 2013].

Incorporating the empirical knowledge from existing field experiments into diagnostic N_2O EF models could improve the accuracy of bottom-up emission estimates and produce upscaling methods from site to region that overcome the incorrect assumption of uniform and constant EF values per crop type. Regionally constant EFs (i.e., $EF = C_i$ for region i) for China's six Agro-Climate Zones were used by *Zhou et al.* [2014], an approach that yields large uncertainties due to significant variations of EFs within each zone. A response curve describing EF as a single linear function (SLF) of nitrogen application rate was used in other studies, i.e., $EF = \Delta EF \cdot N + b$ [*McSwiney and Robertson*, 2005; *Hoben et al.*, 2011; *Shcherbak et al.*, 2014]. Although the SLF model is able to reproduce observed EFs at individual sites [*Shcherbak et al.*, 2014], its performance toward upscaling is generally poor. For example, the R^2 across all site years in *Shcherbak et al.* [2014] is only 0.02 for upland grain crops and 0.04 for paddy rice using fixed values of parameters (i.e., ΔEF and b; Table 1). Conversely, models considering the impacts of environmental variations defined by piecewise EF models (hereafter PM), $EF = \Delta EF \cdot N + b(x_k)$ may better capture the heterogeneity of N_2O EFs and emissions.

The PMs also hold implications for understanding the effects of environmental variations on EF distribution. Applying a random forest algorithm, *Perlman et al.* [2014] found that global N_2O emissions from wheat and maize fields were highly sensitive to SOC and air temperature, and tended to grow exponentially with these two factors. However, the effects on paddy rice and other upland grain crops are still unknown [*Dijkstra et al.*, 2012]. PMs may also provide a tool to help design a N_2O reduction strategy, and these advantages would be greater, at least, if the marginal efficiency of nitrogen fertilizer reductions varies greatly.

Here we explore the heterogeneity of EFs for China's agricultural soils, where the quantity, spatial pattern, and causes of EFs and fluxes remain uncertain compared with developed countries. We propose the PMs (sub section 2.1) and a new version of the Bayesian Recursive Regression Tree (BRRT v2; subsection 2.2) algorithm to identify optimal subfunctions with selected environmental factors and associated subdomains. We then collect N_2O observations with two or more N input levels including a control from inside and outside China, which allows the model calibration and validation (subsection 2.3 and supporting information Text S2). The PM performances are evaluated in the estimates of quantity, spatial patterns, and interannual anomalies of EFs and ΔEF against local N_2O flux observations (subsection 3.1). We also analyzed the differences in predictive accuracy between models with and without varying parameters (subsection 3.1). The predictive accuracy and reliability in upscaling are also assessed using

independent observations out of China (subsection 3.2). Environmental determinants of EFs in China are further quantitatively identified through variable importance and partial dependence analysis (sub section 3.3). Finally, we demonstrate the implications of our models in regional budgets and N reductions in China (subsection 3.4).

2. Methods and Data Set

2.1. PMs for EFs

According to EF-N relationships from 96 field experimental sites (Figure S2), we found that most of them (50/64 for upland grain crops and 29/35 for paddy rice, Figure S1) can be expressed as the linear change in EFs versus N, equivalent to a quadratic growth of N_2O emissions (E) versus N. Contrary to previous works that used the SLF, we propose piecewise linear models (PMs) to account for the shape and heterogeneity of EF:

$$\mathrm{EF}_{\boldsymbol{l}} = \Delta\mathrm{EF}_l(x_k)\cdot N + \mathrm{EF}_l^0(x_k),\ \text{where } x_k \in \Omega_l,\ \forall l \tag{1a}$$

where

$$\mathrm{EF}_l^0(x_k) = \sum_k (b_{kl}\cdot x_k) + c_l, \tag{1b}$$

and l is the index of the subfunction of EFs, $l = 1,\ldots, L$; k is the index of environmental factors, $k = 1,\ldots, K$; and x_k represents the environmental factors applied for any subdomain division Ω_l or regression of each subfunction l, which can be identical, distinct, or overlapped. N is N application rate. $\Delta\mathrm{EF}_l(x_k)$, as the first derivative of EF, indicates the degree of nonlinearity of the emission increase along a gradient of N ($\% \cdot \mathrm{kg}^{-1}\ N_2O\text{-}N \cdot \mathrm{ha}$). $\mathrm{EF}_l^0(x_k)$, as the derivative of E at the point $N = 0$, represents the initial level of EF (%), which is described as an additive linear combination of regression variables x_k and domain-specific coefficients (b_{kl} and c_l).

The above mathematical expression has a biogeochemical basis. First, the model structure is in line with the idea of a Hole-in-the-Pipe (HIP) model [*Davidson et al*., 2000] and the methodology of process-based models [*Li*, 2000; *Haas et al*., 2013; *Bouwman et al*., 2013]. Nitrification and denitrification are primarily described by multiplying three terms: $E = N' \cdot Tr \cdot R + E^0$, where N', Tr, R, and E^0 stand for the available dissolved inorganic nitrogen transformed from N input ($N' = \alpha \cdot N$), the transport rate indicating the residence time of dissolved inorganic nitrogen in root zone (%) [*Van Drecht et al*., 2003], the reaction rate (%), and N_2O emission flux when $N = 0$, respectively. Correspondingly, EF_l in the PMs is equivalent to multiplicative terms $\alpha \cdot Tr \cdot R$. Second, the PMs use a set of linear subfunctions to approximately capture the nonlinear response of EFs to both N and x_k, in order to reflect some of triggering events due to changes in x_k (e.g., water-filled pore space (WFPS) as shown by *Davidson et al*. [2000]). Finally, the selection of environmental factors x_k in the regression reflects their diverse importance on processes Tr and R [*Shcherbak et al*., 2014; *Perlman et al*., 2014].

Eleven environmental factors listed in Table S1 are considered in this study based on the experience of *Bouwman et al*. [2002]. Effective precipitation (as the sum of precipitation and irrigation rate, Precip), total available water capacity (TAWC), and bulk density (BD) for the topsoil are selected to represent the variations of transport rate and WFPS [*Van Drecht et al*., 2003]. Average air temperature (Temp) within measurement period is chosen as a proxy of soil temperature because of their high correlation [*Zheng et al*., 1993]. Soil pH, clay content, soil drainage, TN, and SOC are used to account for O_2 and available C status involved in R [*Bouwman et al*., 2013]. Additionally, fertilizer types and crop types are also selected as environmental factors.

2.2. BRRT v2 Algorithm

The main challenge in calibrating the PMs is to determine the optimal model structure (i.e., L and $x_k \in \Omega_l$) and model coefficients (i.e., $\Delta\mathrm{EF}_l(x_k)$, b_{kl}, c_l) with a minimum cost function. The BRRT v2 proposed algorithm is an updated version of the Bayesian treed model (hereafter BTREED) developed by *Chipman et al*. [2002]. Combining the conditional distribution of EF with prior $p(T)$, the posterior probability $p(T|X,\mathrm{EF})$ in BRRT v2 is calculated as

$$p(T|X,\mathrm{EF}) \propto p(T)p(\mathrm{EF}|X,T), \tag{2}$$

up to a norming constant [*Gelman et al.*, 2003], where X represent environmental factors, i.e., N and x_k in equations (1a) and (1b). T represents a binary tree. Its terminal nodes and splitting rules correspond to the subfunctions, i.e., equations (1a) and (1b), and the subdomains $x_k \in \Omega_l$, respectively. The terms $p(T)$ and $p(\mathrm{EF}|X,T)$ in the BRRT v2 are specified in the BRRT v2 as follows:

$$p(T) = p(I,T)p(\rho|I,T), \tag{3a}$$

$$p(\mathrm{EF}|X,T) = \prod_{l=1}^{L} \int \prod_{m=1}^{M_l} p(\mathrm{EF}_{lm}|x_{klm},\theta_l)p(\theta_l|T)p(x_{kl}|T)\mathrm{d}\theta_l, \tag{3b}$$

where

$$\mathrm{EF}_l|\theta_l \text{ iid} \quad N\left(x_l^T\lambda_l, \sigma_l^2\right), \tag{3c}$$

$$\lambda_l|\sigma_l \quad N\left(\bar{\lambda}_l, \sigma_l^2/a\right), \sigma_l^2 \quad v\omega/\chi_v^2 \tag{3d}$$

$$p(x_{kl}|T) = \frac{C_K^n}{C_K^0 + C_K^1 + \ldots + C_K^K}, \ \forall k = 1,\ldots,n, \tag{3e}$$

and $p(I,T)$ is the probability of terminal node I that is to be resplit, defined as $\tau(1+d_l)^{-\upsilon}$ [*Chipman et al.*, 2002] where d_l is the depth of node I and two hyperparameters $\tau < 1$ and $\upsilon > 0$. The term $p(\rho|I,T)$ is the probability of assigning splitting rule $\rho = \{x_k \le S_k\}$ to terminal node I if it is split, in which x_k is applied as classification variables for subdomain division; $p(\mathrm{EF}_{lm}|x_{klm},\theta_l)$, $p(\theta_l|T)$, and $p(x_{kl}|T)$ are probabilities of EF, regression coefficients, and selection of n of regression variables x_k in terminal I, respectively, in which n is the number of selected x_k. EF_{lm} and x_{klm} denotes the EF and regression variable k of the mth observation in the Ith terminal node, respectively, where $x_{klm} \in X$, $m = 1,2,\ldots, M_l$. θ_l represent a set of regression coefficients λ_l and the variance σ_l of EF in terminal I. All of EF_l are assumed to be independent and identically distributed, in which $x_l^T\lambda_l$ corresponds to equations (1a) and (1b). The ranges of expected values of $\lambda_l = \{\Delta\mathrm{EF}_l(x_k), b_{kl}, c_l\}$ are determined based on the marginal responses of EF to x_k, but we assume that λ_l is normally distributed. The term σ_l is inverse Gaussian distributed with three hyperparameters a, v, and ω. The choice of hyperparameters τ (< 1), υ (> 0), a (= 1 or 3), v (= 3), and ω (= 0.404 or 0.1173) is determined with minimum cost function [*Chipman et al.*, 2002; *Freeman et al.*, 2009]. Detailed methodology and glossary of the BRRT v2 are described in Text S1 and Figure S3, but its three improvements are briefly summarized below.

First, a progressive multirestart stochastic search (hereafter PMRS) algorithm is developed for equations (2) and (3a)–(3e) to accelerate the identification of the optimal T via a minimum number of model executions. Conversely, traditional Bayesian tree-based models [*Chipman et al.*, 2002; *Liu et al.*, 2008; *Jung et al.*, 2009] are so time consuming that it is not easy to traverse the entire optima of trees. The basic strategy of PMRS is to synchronously run a number ($j = 1,\ldots, J$) of restart scenarios of Markov chain sequence of trees and progressively eliminate underperforming trees (e.g., half of trees with higher cost function) before executing subsequent running stages, until the tree with optimal L, $x_k \in \Omega_l$, $\lambda_l = (\Delta\mathrm{EF}, b_{kl}, c_l)$, and σ_l is identified in final running stages with a minimum cost function. In the process of PMRS, each tree in Markov chain sequence is searched by Metropolis-Hastings (MH) algorithm [*Chib and Greenberg*, 1995]. The cost function in BRRT v2 that is minimized is the Bayesian Information Criterion (BIC) [*Jung et al.*, 2009].

Second, a new deterministic split or pruning operator (GREEDY), finding the locally optimal tree, is designed and directly combined into the previous four-mode stochastic search of BTREED model. This update avoids to nudging to local subdomains when processing the transition from old tree T^i to the new one T^{i+1} in the MH search. If implementing GREEDY, the terminal node $\hat{l}$ of T^i can be split if the residual sum of squares of its two child nodes is minimum among all terminal nodes of T^{i+1} and smaller than that of entire node $\hat{l}$, otherwise, an intermediate node is pruned upward into a terminal node when the complexity cost reaches a minimum [*Breiman et al.*, 1984].

Third, the abovementioned selection of regression variables in equation (1b) for each terminal node is then launched when one of five modes has been chosen in the MH search. This process is achieved through both random and deterministic approaches. First, regression variables are randomly selected based on prior $p(x_{kl}|T)$; Second, the randomly selected x_k is further screened by stepwise forward regression. The forms of EF_l and $p(\mathrm{EF}|X,T)$ are updated accordingly. Contrary to the BTREED [*Chipman et al.*, 2002], variable selection helps reduce the number of redundant x_k used in equation (1b) for individual terminal nodes.

2.3. Data Set

For training piecewise EF models, we collected N_2O measurements and the corresponding x_k in China's agricultural soils from 153 peer-reviewed studies including with 178 zero-N application. After data screening (described in Text S2 and Table S3), this data set comprised 732 site years (521 for upland grain crops and 211 for paddy rice) at 96 sites from 1994 to 2013. It covers most major cereal-production areas in China and the phase space of environmental conditions (Figure S3). We used all site years in the original studies, averaged by replicates if necessary. Missing values (less than 200 site years) of soil attributes or climate within measurement period are supplemented by the 1 km Harmonized World Soil Database (HWSD) v1.2 [*FAO/IIASA/ISRIC/ISSCAS/JRC*, 2012] or by climate data of the nearest stations from the China Meteorological Data Sharing Service System (http://cdc.cma.gov.cn).

The PMs calibrated by observations from China are validated by independent observations from outside China. Specifically, 445 site years (including 124 records at zero-N control) from 56 sites (Figure S4) that satisfy our selection criteria (see Text S2) are extracted from *Akiyama et al*. [2005], *Stehfest and Bouwman* [2006], and *Shcherbak et al*. [2014], where parts of x_k in their data set are supplemented from original articles.

PMs are also applied to simulate the spatial distribution of fertilizer-induced N_2O emissions over China arable lands in 2008 at a 1 km scale. The forcing data set is prepared as follows: (i) a 1 km land use map in 2010 with soil attributes (BD, TAWC, clay content, soil drainage, pH, TN, and SOC) is directly extracted from *Liu et al*. [2014] and HWSD v1.2, which are assumed to represent the target year 2008; (ii) county-level data of the annual amounts of synthetic fertilizers and manure applied in 2008 are obtained for 2884 political units from *Zhou et al*. [2014], and disaggregated into 1 km maps based on the above cropland distribution; (iii) annual Precip and Temp in 2008 are obtained from 0.25° data set of TRMM 3B42RT [*Huffman et al*., 2010] and Climate Research Unit (CRU TS v. 3.22) [*Harris et al*., 2014], respectively, and then downscaled based on 1 km WorldClim v1.4 [*Hijmans et al*., 2005]; and (iv) 5 min percentages of area actually irrigated (δ) are extracted from FAO Global Map of Irrigation Areas v5.0 (GMIA) [*Siebert et al*., 2013] over China and resampled it into 1 km grid cells, and further bias corrected based on municipal-level data set of actual irrigation area in 2008 from 34 provincial statistical registers (PSRs) in China. Actual irrigation rate per grid cell is finally calculated as the product of municipal irrigation rate per area and δ, where the former can also be obtained from the PSR data set.

3. Results and Discussion

3.1. Model Accuracy in Calibration

According to a sensitivity analysis of BRRT v2 to hyperparameters [*Freeman et al*., 2009], the minimum BIC exists at $\tau = 0.95$, $\upsilon = 1.0$, $a = 1$, and $\omega = 0.1173$. Additionally, fivefold cross validation was applied to avoid overfitting in model calibration. The BRRT v2, initialized with 20 restarts of 500 iterations per stage, then found the 10- and 7-node trees for upland grain crops and paddy rice with minimum BIC being -583 and -381 respectively, after 20,500 iterations ($= 500 \times [20 + 10 + 5 + 3 + 2 + 1]$) of six running stages. Finally, the relevant x_k for subdomain divisions were identified to be crop type, fertilizer type, and Temp for upland grain crops and fertilizer type and Precip for paddy rice. The regression variables are Precip, Temp, soil pH, *N* for upland grain crops and Temp, clay content, soil TN, and *N* for paddy rice, where the corresponding standard errors and *p* values are listed in Table S3.

Figures 1a and 1e show that the data-driven PMs are able to explain 84% and 91% of the variances for upland grain crops and paddy rice (averaged from fivefold cross validation in supporting information Table S2), respectively. The mean squared errors (MSEs) of simulated EFs were 0.1% for upland grain crops and 0.03% for paddy rice, indicating very low bias in the models. We also found that few simulated EFs differ significantly from observations for upland grain crops (solid blue circles in Figure 1a). For the point #1 in Figure 1a [*Liu et al*., 2010], N_2O emissions, including a peak flux during the fallow period of rice, were improperly accounted for in the following wheat-growing season, eventually enlarging the observed EF. For the point #2 [*Zhang et al*., 2012], the zero-N application plot was managed as bare soil, which possibly lowers background N_2O flux and increases EF [*Ussiri and Lal*, 2012]. Two other larger discrepancies between PM results and observations shown in Figure 1a are attributed to the fact that the PMs do not account for the effects of different percentages of manure in total N inputs (point #3 in Figure 1a)

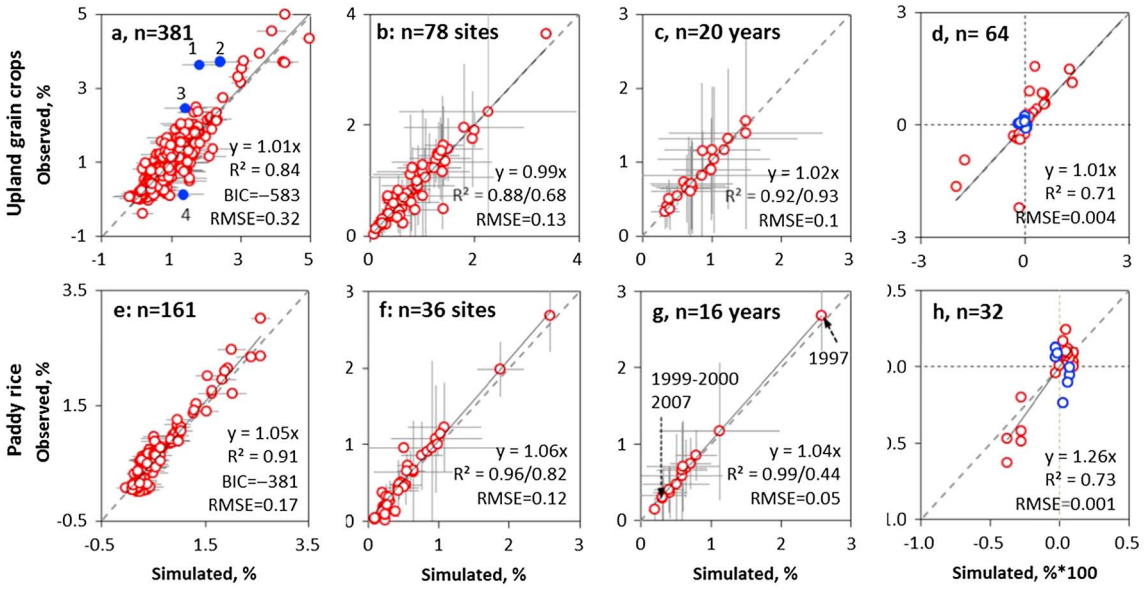

Figure 1. Calibration of EF and ΔEF for upland grain crops and paddy rice in China.(a or e) Modeled and observed EFs of all site years, (b or f) modeled and observed EFs averaged by sites and the associated standard errors (SEs, gray error bars), where the R^2 values before and after slash are for the means and SEs of EFs, respectively, (c or g) Modeled and observed EFs averaged by years and the associated SEs, and (d or h) modeled and observed ΔEFs of all site years. The full data set is illustrated as red open circles, while the estimates with disagreement in the magnitude of EFs and signs of ΔEFs between simulated and observed results are represented as solid and open blue circles, respectively. Four outliers in Figure 1a are marked by the number 1 [*Liu et al.*, 2010], 2 [*Zhang et al.*, 2012], 3 [*Yang et al.*, 2007], and 4 [*Yu et al.*, 1995]. All error bars for EFs are 1 SE. The slope, R^2, BIC, and the square root of MSE (RMSE) are indicated in the insets at the bottom right of each panel.

[*Yang et al.*, 2007] or the changes in illumination intensity (point #4 in Figure 1a) [*Yu et al.*, 1995] on the N_2O flux. Without these four records, R^2 for upland grain crops increases from 0.86 to 0.89 and root-mean-square error (RMSE) decreases to 0.2 across upland crops.

A higher R^2 (>0.88) and lower RMSE of the simulated EFs in Figures 1b, 1c, 1f, and 1g compared to Figures 1a and 1e show that the PMs can precisely reproduce spatial patterns, interannual anomalies, and the associated variations, except for the temporal variations within 1997–2000 and 2007 for paddy rice (Figure 1g). Model performance for ΔEFs is also examined from sites fertilized at three or more N input levels in Figures 1d and 1h. Contrary to the global results of *Shcherbak et al.* [2014], the number of negative ΔEFs in China (41% for upland grain crops and 44% for paddy rice) is comparable to the number of positive values (Figure 2). In principle, reliable calibrations of ΔEF depend on the accuracies of both individual EFs and their range of variations within each group. A BIC-oriented model calibration leads to a limited number of ΔEFs, which makes it more difficult to accurately reproduce all observed ΔEFs. However, the accuracy in ΔEFs ($R^2 = 0.71$) is acceptable, because (i) the differences of larger positive or smaller negative ΔEFs from the observations are relatively low and their signs are correctly captured; (ii) yet a few of simulated ΔEFs disagree in signs with observed results (open blue circles in Figures 1d and 1h), they are relatively close to zero.

We then assess the differences between the results of the PMs and the classical IPCC Tier 1 model, based upon constant crop-specific EF [*IPCC*, 2006; *Gao et al.*, 2011; *Lu et al.*, 2006; *Zou et al.*, 2009; *Wang et al.*, 2011b], the regionally constant EF model [*Zhou et al.*, 2014], the SLF model [*Hoben et al.*, 2011; *Shcherbak et al.*, 2014], and the Residual Maximum Likelihood approach [*Bouwman et al.*, 2002; *Akiyama et al.*, 2005; *Stehfest and Bouwman*, 2006]. Performance statistics in Table 1 illustrate that the PM results are superior to all parameter-fixed models for the full modeling domain. To unveil the advantage of the PMs, we also compared the results of BTREED model [*Chipman et al.*, 2002] with the same number of restarts and iterations (20,500) and the values of hyperparameters. In this sensitivity test, the BTREED shows a lower R^2, higher RMSE, and a higher BIC for both upland grain crops and rice (Table 1). This result can be explained by the three improvements of the new BRRT v2. Ability in parameter selection of five modes reduced the redundant environmental variables for the regression, and the PMRS algorithm with the new GREEDY mode increases the possibility of traversing the entire optima of trees while avoiding ineffective searching in local regions.

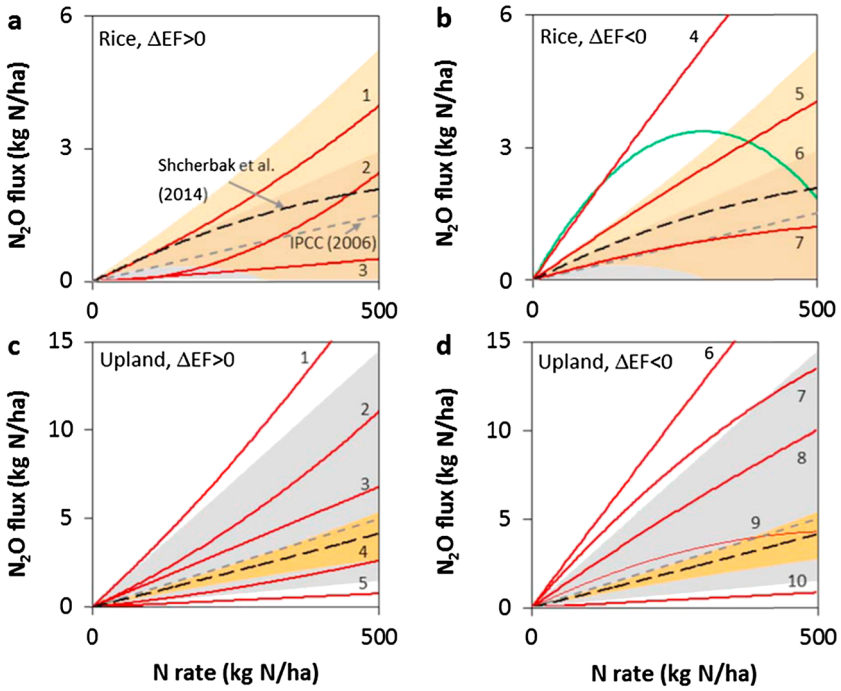

Figure 2. (a–d) Comparison of our E-N relationship with IPCC Tier 1 (gray dashed lines) and SLF model of *Shcherbak et al.* [2014] for all site years (black dashed lines). The curve with minimum ΔEF (= − 0.0037% · kg^{-1} N_2O-N · ha) is shown in green solid line in Figure 2b. The digits above solid lines indicate the number of subfunctions. The 95% confidence intervals (CIs) for IPCC Tier 1 and SLF models are shown in gray and orange shaded areas, respectively. IPCC Tier 1 95% CIs are 0.3–3% for upland grain crops and 0–0.6% for paddy rice.

The better performances of the PMs compared to other models are attributed to its explicit accounting of heterogeneity in EFs. *E-N* relationships corresponding to the subfunctions of EFs are illustrated in Figure 2 for upland grain crops and paddy rice under positive or negative ΔEFs. The diagnostic of negative ΔEFs (Figures 2b and 2d) suggests that activity or efficiency of nitrifier and denitrifier communities may reach thresholds and further stabilize around these thresholds, when *N* inputs exceed crop requirements [*Ju et al.*, 2009; *Tatti et al.*, 2013]. However, the strange decrease in *E* (as the green line in Figure 2b and ΔEF = −0.0037% · kg^{-1} N_2O-N · ha) does not have a satisfactory theoretical explanation, though this type of trend was occasionally observed [*van Groenigen et al.*, 2004; *Hoogendoorn et al.*, 2008; *Iqbal*, 2009; *Wang et al.*, 2011a; *Zhang et al.*, 2012; *Signor et al.*, 2013; *Zhou et al.*, 2013]. Conversely, it is impossible for constant, regionally constant, or SLF EF models to capture these variations of observed EFs across China (Figure 2).

3.2. Model Reliability Validated by Independent Observations

Having shown the better performance of PMs, we focus now on model reliability through cross validation by independent data. Figure 3 demonstrates that the PMs calibrated by China's observations are also able to capture the variations of EFs when the sites have a phase space of predictors similar to China ($R^2 = 0.75$ for both upland grain crops and paddy rice). This result provides additional confidence on the predictive capabilities of PMs, meaning that the same models could be applied to predict EF heterogeneities in regions that have a phase space of environmental factors similar to China. However, ~10% of the cross-validation observations (35 site years) could not be reproduced by our models because of the sites whose x_k are not present in China's data set (or subject to extrapolation; Figure 3). The fact that most N_2O field experiments in China are within temperate or subtropical zones results in this situation outside this climate space, because climates in low- or high-latitude regions (e.g., Canada, Spain, Finland, Southeast Asia for upland soils, and Philippines for paddy rice that corresponds to the black circles in Figure 3; see also Figure S5) are outside the phase space considered for model calibration in China. We then check the occurrence of this situation in China. Only a small fraction (~9%) of the pixels is, however, subject to this

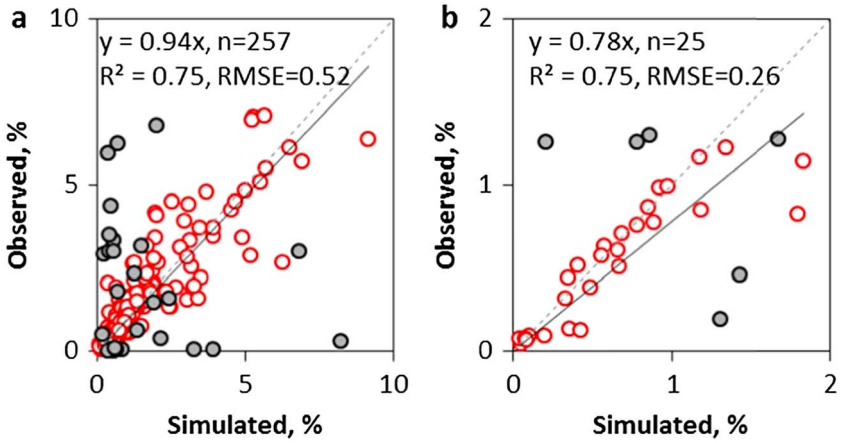

Figure 3. Model cross validations by N_2O measurements outside China for (a) upland grain crops, and (b) paddy rice. The fluxes simulated at sites whose environmental conditions are or are not captured by China's data set are illustrated as red open circle or black solid circle, respectively.

extrapolation for China in 2008. Those are agricultural soils in the northern borders of China (>45°N) and in the Sichuan Basin, where reaction velocity and biogeochemistry of N are not adequately captured with the data used to calibrate the model. To avoid extrapolation or enhance extrapolation capacity, the PMs would need to be recalibrated using more observations from these regions, which is an additional step that can be taken in the future.

3.3. Environmental Determinants of EF Distribution

The relative importance of the identified x_k on EFs is further quantified in this section. Importance is defined as the magnitude of the increase in MSE when x_k is randomly permuted [*Perlman et al.*, 2014]. For both upland grain crops and paddy rice, climate alone can explain 69% and 85% of the variations in EF distribution across China, where Temp and Precip stand out as the single most important determinants (Figures 4a and 4b). This finding indicates that soil temperature and moisture (through accumulated precipitation and irrigation as well as temperature-controlled evapotranspiration demand) both

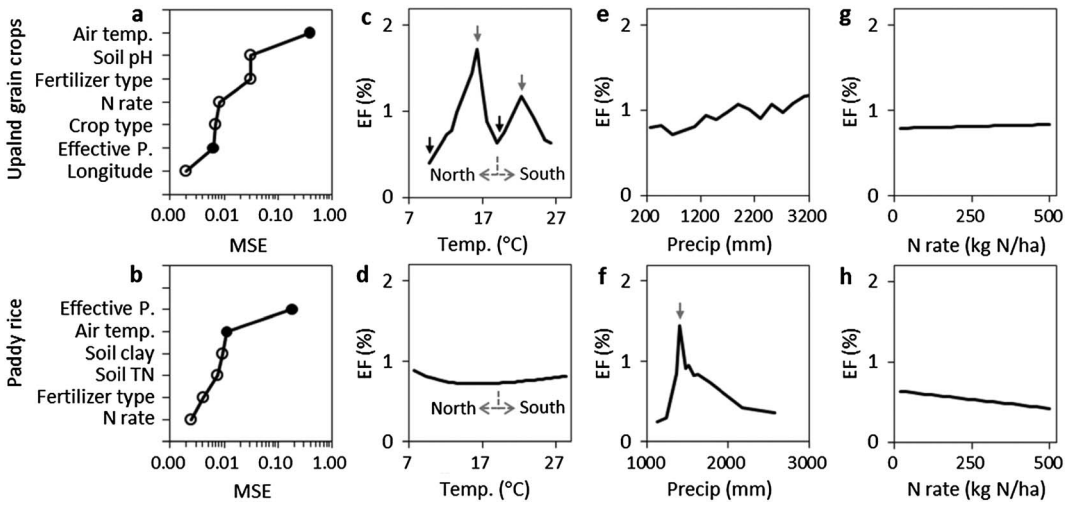

Figure 4. (a and b) Variable importance and (c–h) partial dependence of EF as a function of environmental factors. Importance is defined as the magnitude of the increase in MSE when x_k is randomly permuted, while partial dependence is defined as the response of EF to a given x_k by statistically controlling for the average effect of all other environmental factors. EFs in Figures 4c–4f are calculated for the same reference N application rate of 200 kg N ha^{-1}. Temperature and precipitation optima (T_{opt}) are indicated by gray arrows, while the minimum threshold temperatures (T_{opt}) are indicated by black arrows.

regulate the reaction rates of C and N cycles and the occurrences of soil anaerobic conditions that promote higher EFs. Soil pH is then ranked second for upland grain crops, which confirms the observations that soil acidification further enhanced the sensitivity of the N_2O EFs [*Ju et al*., 2009; *Guo et al*., 2010].

We also used the PM results to diagnose the sensitivity of EF to Temp and Precip through a partial dependence analysis. Partial dependence is defined as the marginal response of EF to a given x_k by statistically controlling for the average effect of all other environmental factors. The results shown in Figures 4c–4f depict the modeled EF for different values of Temp and Precip for each of the records in the model training data.

For the partial dependence of temperature (Figures 4c and 4d), the EF of upland grain crops increases exponentially from 0.4% to 1.7% until reaching an optimum temperature (T_{opt}) of ~16°C (Figure 4c), followed by an abrupt decline. Above ~19°C, the EF rises again to 1.1% until it approaches the second optima (~22.5°C), and finally decreases to 0.6% at ~26.3°C (Figure 4c). This shape with two maxima is distinct from monotonic increases previously found at specific sites (Figure S1) or in global models [*Perlman et al*., 2014]. However, multiple EF optima were detected in the manipulation experiments, when analyzing EFs across diverse climates or site characteristics [*Farquharson and Baldock*, 2008; *Singurindy et al*., 2009; *Kurganova and de Gerenyu*, 2010; *Dijkstra et al*., 2012]. Thus, the complex two-peaked curve in Figure 4c could be interpreted by the occurrence of optima and its adaptation to different climate zones. First, elevated temperature can directly stimulate microbial processes which cascade Nr providing substrate for denitrification, eventually enhancing N_2O evasions [*Butterbach-Bahl et al*., 2013]. However, these positive effects of a temperature increase can be offset by its opposite effects [*Dijkstra et al*., 2012]. When exceeding the optima, increasing temperature can boost plant N uptake, N volatilization [*Skjøth and Geels*, 2013], cause rapid soil drying [*Bijoor et al*., 2008], or decrease the N_2O:N_2 ratio [*Troy and Tang*, 2011], which altogether decreases the fraction of soil N lost as N_2O. Second, two successive optimum functions, roughly divided at ~19°C (Figure 4c), suggest two separate response curves for northern (119 observations from 34 sites) and southern China (262 observations from 37 sites) according to the spatial distribution of experimental sites in training data set (Figure S6). Regional studies in forest ecosystems [*Breuer and Butterbach-Bahl*, 2005] indicated that microbial communities in upland soils may adapt or acclimate to ambient low or high temperature, resulting in individual temperature maxima in northern and southern China. Compared with southern China, the temperature response function of EFs in northern China has larger maxima relative to minimum threshold temperatures (T_{min}; i.e., the distance between T_{opt} and T_{min}; Figure 4c). The adaptive optimum temperature functions applied for instance in the process-based model DAYCENT [*Parton et al*., 2001; *Del Grosso et al*., 2009] would thus be better choice than exponential or Arrhenius type functions to simulate the EF distribution for China's upland soils. Opposite to upland soils, it is important to note that the temperature dependency of EF for paddy rice is quite flat (Figure 4d) across a similar temperature range than upland soils. This finding may be explained by the fact that positive and negative effects of elevated temperature may be compensated by each other [*Dijkstra et al*., 2012], resulting into an overall small temperature sensitivity of EF for paddy rice.

For precipitation, EF can be described as a single optimum function of Precip for paddy rice (Figure 4f). EF grows rapidly with Precip starting at 1100 mm and reaches a peak of 1.5% at Precip ≈ 1400 mm, and then falls down slowly for the range of 1400 ~ 2,580 mm. This trend could be well explained by the HIP conceptual model of *Davidson et al*. [2000], which found N_2O emissions peak at 70–90% WFPS. However, the shape of the curve shown in Figure 4f looks like a positively-skew Laplace distribution, unlike the negatively-skew EF-WFPS relationship given by *Davidson et al*. [2000]. This result may be explained by the fact that intensive irrigation is common for rice in China [*Zou et al*., 2009], which increases the occurrence probability of being near or fully saturated in most of the experimental sites. Thus, additional field measurements with less Precip in the future would be needed to confirm the precipitation sensitivity curve for paddy rice. For upland grain crops, a threshold of 70–90% WFPS is not supported by the calibrated PM results. Figure 4e indicates that EF rather increases fluctuantly with Precip. These upland soils in China may rarely reach optimum moisture conditions even under high irrigation rates.

Additionally, we discussed the differences between the sensitivity of EF due to N application rate and environmental factors. The EFs of upland grain crops increase slightly from 0.79% to 0.83% along the

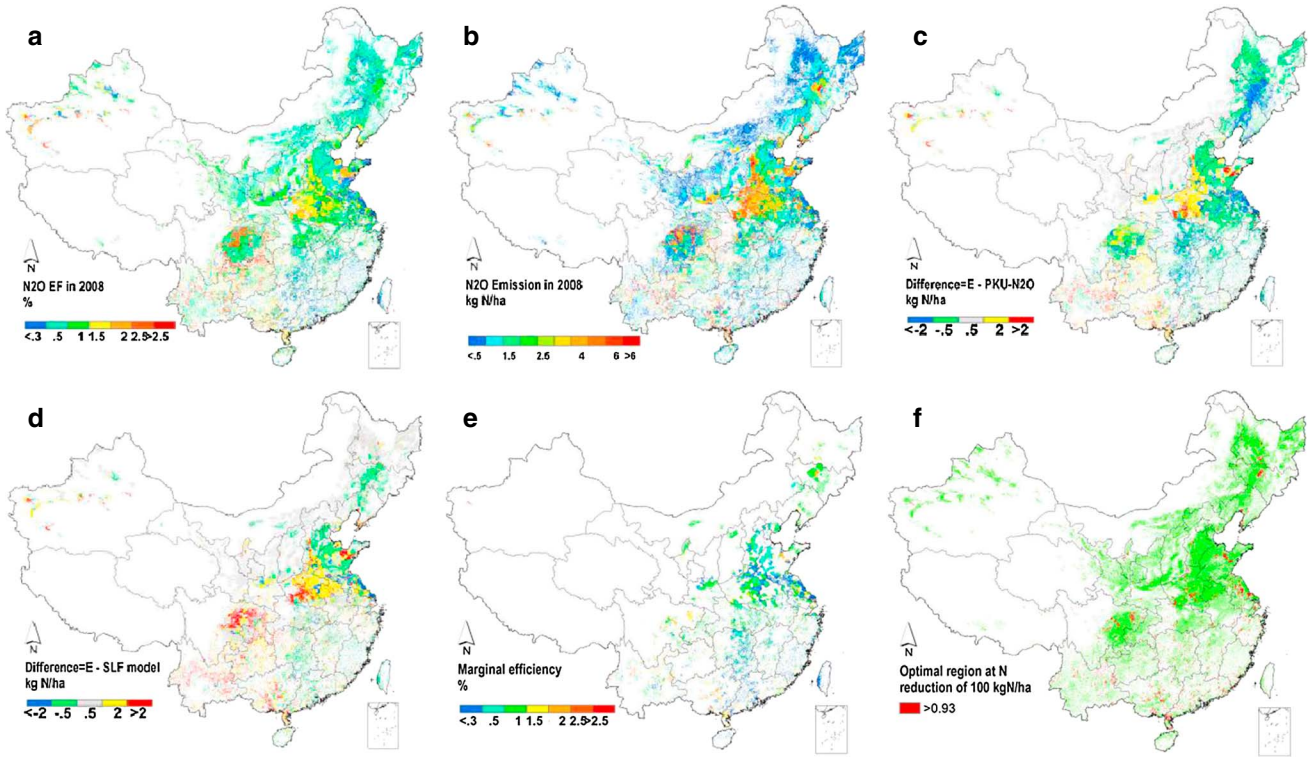

Figure 5. One kilometer spatial patterns of N_2O EFs and emissions, differences with other EF models, and implications in N_2O reductions. (a) N_2O EFs in 2008, (b) N_2O emissions in 2008, (c) differences with regionally constant EF model, (d) differences with SLF model, (e) marginal efficiency at a N fertilizer reduction of 100 kg N ha^{-1}, (f) the lowered N_2O emissions that are larger than 0.93 kg N_2O-N ha^{-1} (red). The light green in Figure 5e represents cropland.

gradient of N application rates (0–500 kg^{-1} N · ha; Figure 4g), while the EFs of paddy rice decrease from 0.63% to 0.42% (Figure 4h). Contrary to N application rate, the EFs are more sensitive to Temp or Precip (Figures 4c and 4f). In other word, although EFs changed linearly with N application rates at most individual sites where environmental factors were almost constant within the measurement period (Figure S1), the magnitude and spatial distribution of EFs are found to be much more determined by climate factors, highlighting the need for upscaling methods that account for environmental factors than just N application rate.

3.4. Implications on Emission Inventory and N Reductions

Based on gridded data set of identified environmental factors x_k, fertilizer-induced N_2O emissions are estimated over the territory of China by the PMs, and uncertainties from five different sources are deliberately considered (1) N application rates, (2) environmental factors, (3) measurement errors, (4) parameter estimates, and (5) errors due to extrapolation. The detail of uncertainty analysis is described in Text S3. Our estimate of the fertilizer-induced N_2O emission from China is of 323.8 ± 60.3 Gg N_2O-N yr^{-1} (1σ), with 272.6 ± 49.1 for upland grain crops and 51.2 ± 11.3 Gg N_2O-N yr^{-1} for paddy rice. The corresponding average EFs are $0.84 \pm 0.18\%$ and $0.65 \pm 0.14\%$. The latter value for rice is 1.2 times larger than the IPCC Tier 1 default value. The IPCC Tier 1-derived estimates of EFs (1% or 0.3%) result into a slight overestimation of N_2O emissions for upland soils and a significant underestimation for paddy rice emissions (Table 1). We also found significant underestimation (overestimation) for upland crops (paddy rice) of N_2O emissions for models using regionally constant or SLF EF models compared to PMs, probably because those models do not account for the effects of spatial variations or seasonality of x_k on EFs (Table 1).

The constant, regionally constant, and SLF EF models result in very different N_2O emission spatial patterns in China compared to the map derived from the PMs. In particular, EFs in the year 2008 simulated by PMs vary greatly across China (Figure 5a). The highest values (>2%) are found in the southwestern China, the north

China Plain, and upland fields around the Taklamakan Desert, whereas the lowest values (<0.3%) are in northern Jiangsu and southern China (Figure S7). The spatial pattern of N_2O emissions (Figure 5b) is similar to the one of EFs (Figure 5a), but hot spots of N_2O emissions (>6 N_2O-N · ha^{-1}) are amplified in high-EF regions, where most cereal and livestock production in China occurs [*Zhou et al*., 2014]. High-emission densities (>4 kg N_2O-N · ha^{-1}) are also found in the central part of northeastern China and several counties discretely distributed in Jiangsu and Shandong provinces (Figure S7).

The absolute differences (AD) between regional EF models (E_2) and our estimates (E_1) of N_2O emissions are also assessed, defined as $AD = E_1 - E_2$. Compared to regionally constant EF models [*Zhou et al*., 2014], our estimates are ~1.5 kg N_2O-N ha^{-1} higher in Henan, Yunnan, and Guangxi, but ~2 kg N_2O-N ha^{-1} lower in the Northeast Plain and northern Jiangsu (Figures 5c and S7). These findings indicate that EFs, averaged from different experiments that define the constant EF or regionally constant EF models, do not capture the heterogeneity at local scales. EFs of SLF model are relatively closer to our estimates in low-emission-density regions (Figure 5d), where EFs are generally determined by the term $\Delta EF_l(x_k) \cdot N$. However, underestimations are significant in the Sichuan Basin, the Yunnan-Guizhou Plateau, and the North China Plain (Figure S7), where soils are moderately acidic, leading to higher $EF_l^0(x_k)$.

Additionally, the PMs could be easily applied to identify regions that constitute the best opportunities to implement effective N_2O reduction strategies in China. We define the mitigation potential of N_2O emissions by the difference between the baseline value E_B and the value E_R with reduced input ΔN set to 100 kg N · ha^{-1}. To ensure no yield loss from suboptimal N applications, the remaining N application rate ($N - \Delta N$) needs to exceed the crop requirements (~200 kg · ha^{-1} for upland grain crops and ~100 kg · ha^{-1} for paddy rice) [*Roy et al*., 2006; *Ju et al*., 2009]. The term "potential" here means no consideration of costs, technical feasibility, and other trade-offs. The marginal efficiency of the mitigation (η_R) is deduced as

$$\eta_R = (E_B - E_R)/\Delta N = EF + (N - \Delta N) \cdot \Delta EF(x_k). \quad (4)$$

Figure 5e shows that few pixels have η_R values smaller than EFs, which means that hot spots of η_R (>1%) are partly distributed in the region where $\Delta EF < 0$. Approximately 50% of the N_2O mitigation potential originates from only 22% of China's agricultural soils. Regions with the highest mitigation potential include upland fields in southern China, such as Guangxi, Yunnan, Guangdong, and the Northern Sichuan Basin (Figure 5f). These results suggest that mitigation could be effectively implemented in these areas, considering only a maximization of the amount of achievable emission reduction but not accounting for economic trade-offs and cobenefits. However, the η_R estimated by the constant EF models is constant for all lands and reduction scenarios. Although the SLF model reflects part of heterogeneity of the EF, it is difficult to avoid underestimating or overestimating η_R, as it is similar with the EF.

4. Conclusion

We presented a new piecewise linear modeling approach to simulate the complex and poorly understood spatial patterns of N_2O emission factors. The associated BRRT v2 algorithm developed for that purpose captures the observed heterogeneity of EF across China. The models are of higher accuracy and reliability compared to other EF determinations that ignore the impacts of spatial gradients in environmental factors. The PM models are able to (1) quantify the effects of climate as important determinants in regulating the EF distribution across China, (2) simulate their effects on a large scale, and (3) provide high-resolution N_2O emission maps and a tool to map the most suitable regions for mitigation in terms of amount achievable. We conclude that (1) the piecewise EF models and BRRT v2 may be powerful enough to perform regional or global upscaling of the N_2O flux and similar works (water, CO_2, CH_4, gross primary production, etc), if having sufficient and representative observations (e.g., FLUXNET), (2) the models calibrated by China's observations are also applicable for other countries or regions that are subject to interpolation, and (3) attention to the quality, detail, and resolution of climates is much more important than other forcing data for N_2O EFs estimation in China.

We realize that it is inappropriate to substitute piecewise EF models for IPCC Tier 1 defaults directly. According to model inference, our estimated EF can only reflect N_2O emissions induced by inputs of new nitrogen (i.e., fertilizers or N depositions), not residual nitrogen (e.g., crop residues, soil mineralization, and

managed organic soils) [*Novoa and Tejeda*, 2006]. Thus, we suggest that EFs and emissions for new and residual nitrogen should be revised as product of fertilizer-induced EFs in equations (1a) and (1b) and a correction coefficient *r*; however, how to determine *r* becomes another question to be undertaken by future studies.

Acknowledgments
Funding for this study was provided by the National Natural Science Foundation of China (41201077), the Research Fund for the Doctoral Program of Higher Education of China (20120001120129), 111 Project (B14001), China Scholarship Council Program (201308110277), and NSF (NSF 12-532). We appreciated HWSD, CRU, IGSNRR, and GMIA teams for providing soil, climate, land use, and irrigation data set, and authors who measured, analyzed, and published data of N_2O used here. The data to support this article and China's 1 km N_2O emission inventory are available by contacting the corresponding author (zhouf@pku.edu.cn).

References

Akiyama, H., K. Yagi, and X. Y. Yan (2005), Direct N_2O emissions from rice paddy fields: Summary of available data, *Global Biogeochem. Cycles*, *19*, GB1005, doi:10.1029/2004GB002378.

Bijoor, N. S., C. I. Czimczik, D. E. Pataki, and S. A. Billings (2008), Effects of temperature and fertilization on nitrogen cycling and community composition of an urban lawn, *Global Change Biol.*, *14*(9), 2119–2131.

Bouwman, A. F., L. J. M. Boumans, and N. H. Batjes (2002), Modeling global annual N_2O and NO emissions from fertilized fields, *Global Biogeochem. Cycles*, *16*(4), 1080, doi:10.1029/2001GB001812.

Bouwman, A. F., A. H. W. Beusen, J. Griffioen, J. W. Van Groenigen, M. M. Hefting, O. Oenema, P. J. T. M. Van Puijenbroek, S. Seitzinger, C. P. Slomp, and E. Stehfest (2013), Global trends and uncertainties in terrestrial denitrification and N_2O emissions, *Philos. Trans. R. Soc., B*, *368*, doi:10.1098/rstb.2013.0112.

Breiman, L., J. H. Friedman, R. A. Olshen, and C. G. Stone (1984), *Classification and Regression Trees*, Wadsworth International Group, Belmont, Calif.

Breuer, L., and K. Butterbach-Bahl (2005), Local temperature optimum of N_2O production rates in tropical rain forest soils of Australia, *Aust. J. Soil Res.*, *43*(6), 689–694.

Butterbach-Bahl, K., E. M. Baggs, M. Dannenmann, R. Kiese, and S. Zechmeister-Boltenstern (2013), Nitrous oxide emissions from soils: How well do we understand the processes and their controls?, *Philos. Trans. R. Soc., B*, *368*, doi:10.1098/rstb.2013.0122.

Chib, S., and E. Greenberg (1995), Understanding the metropolis-hastings algorithm, *The American Statistician*, *49*(4), 327–335.

Chipman, H. A., E. I. George, and R. E. McCulloch (2002), Bayesian treed models, *Mach. Learn.*, *48*(1–3), 299–320.

Davidson, E. A., M. Keller, H. E. Erickson, L. V. Verchot, and E. Veldkamp (2000), Testing a conceptual model of soil emissions of nitrous and nitric oxides, *BioScience*, *50*(8), 667–680.

Decock, C. (2014), Mitigating nitrous oxide emissions from corn cropping systems in the Midwestern US: Potential and data gaps, *Environ. Sci. Technol.*, *48*(8), 4247–4256.

Del Grosso, S. J., D. S. Ojima, W. J. Parton, E. Stehfest, M. Heistermann, B. DeAngelo, and S. Rose (2009), Global scale DAYCENT model analysis of greenhouse gas emissions and mitigation strategies for cropped soils, *Global Planet. Change*, *67*(1–2), 44–50.

Dijkstra, F. A., S. A. Prior, G. B. Runion, H. A. Torbert, H. Q. Tian, C. Q. Lu, and R. T. Venterea (2012), Effects of elevated carbon dioxide and increased temperature on methane and nitrous oxide fluxes: Evidence from field experiments, *Front. Ecol. Environ.*, *10*(10), 520–527.

Emission Database for Global Atmospheric Research (2014), Global emissions EDGAR v4.2 FT2010, edited.

FAO/IIASA/ISRIC/ISSCAS/JRC (2012), Harmonized World Soil Database (version 1.2) FAO, Rome, Italy and IIASA, Laxenburg, Austria.

Farquharson, R., and J. Baldock (2008), Concepts in modelling N_2O emissions from land use, *Plant Soil*, *309*(1–2), 147–167.

Freeman, A. M., E. C. Lamon, and C. A. Stow (2009), Nutrient criteria for lakes, ponds, and reservoirs: A Bayesian TREED model approach, *Ecol. Modell.*, *220*(5), 630–639.

Gao, B., X. T. Ju, Q. Zhang, P. Christie, and F. S. Zhang (2011), New estimates of direct N_2O emissions from Chinese croplands from 1980 to 2007 using localized emission factors, *Biogeosciences*, *8*(10), 3011–3024.

Gelman, A., J. B. Carlin, H. S. Stern, and D. B. Rubin (2003), *Bayesian Data Analysis*, Chapman and Hall, New York.

Grace, P. R., G. P. Robertson, N. Millar, M. Colunga-Garcia, B. Basso, S. H. Gage, and J. Hoben (2011), The contribution of maize cropping in the Midwest USA to global warming: A regional estimate, *Agric. Syst.*, *104*(3), 292–296.

Guo, J. H., X. J. Liu, Y. Zhang, J. L. Shen, W. X. Han, W. F. Zhang, P. Christie, K. W. T. Goulding, P. M. Vitousek, and F. S. Zhang (2010), Significant acidification in major Chinese croplands, *Science*, *327*(5968), 1008–1010.

Haas, E., S. Klatt, A. Frohlich, P. Kraft, C. Werner, R. Kiese, R. Grote, L. Breuer, and K. Butterbach-Bahl (2013), LandscapeDNDC: A process model for simulation of biosphere-atmosphere-hydrosphere exchange processes at site and regional scale, *Landscape Ecol.*, *28*(4), 615–636.

Harris, I., P. D. Jones, T. J. Osborn, and D. H. Lister (2014), Updated high-resolution grids of monthly climatic observations–The CRU TS3.10 Dataset, *Int. J. Climatol.*, *34*, 623–642.

Hijmans, R. J., S. E. Cameron, J. L. Parra, P. G. Jones, and A. Jarvis (2005), Very high resolution interpolated climate surfaces for global land areas, *Int. J. Climatol.*, *25*(15), 1965–1978.

Hoben, J. P., R. J. Gehl, N. Millar, P. R. Grace, and G. P. Robertson (2011), Nonlinear nitrous oxide (N_2O) response to nitrogen fertilizer in on-farm corn crops of the US Midwest, *Global Change Biol.*, *17*(2), 1140–1152.

Hoogendoorn, C. J., C. A. M. de Klein, A. J. Rutherford, S. Letica, and B. P. Devantier (2008), The effect of increasing rates of nitrogen fertiliser and a nitrification inhibitor on nitrous oxide emissions from urine patches on sheep grazed hill country pasture, *Aust. J. Exp. Agric.*, *48*(1–2), 147–151.

Huffman, G. J., R. F. Adler, D. T. Bolvin, and E. J. Nelkin (2010), The TRMM multi-satellite precipitation analysis (TMPA), in *Satellite Rainfall Applications for Surface Hydrology*, edited by F. Hossain and M. Gebremichael, pp. 3–22, Springer, Dordrecht, Netherlands.

Intergovernmental Panel on Climate Change (IPCC) (2006), *2006 IPCC Guidelines for National Greenhouse Gas Inventories, National Greenhouse Gas Inventories Programme*, IGES, Japan.

Iqbal, M. T. (2009), Effects of nitrogen and phosphorous fertilisation on nitrous oxide emission and nitrogen loss in an irrigated rice field, *Malays. J. Soil Sci.*, *13*, 105–117.

Ju, X. T., et al. (2009), Reducing environmental risk by improving N management in intensive Chinese agricultural systems, *Proc. Natl. Acad. Sci. U.S.A.*, *106*(9), 3041–3046.

Jung, M., M. Reichstein, and A. Bondeau (2009), Towards global empirical upscaling of FLUXNET eddy covariance observations: Validation of a model tree ensemble approach using a biosphere model, *Biogeosciences*, *6*(10), 2001–2013.

Kim, D. G., G. Hernandez-Ramirez, and D. Giltrap (2013), Linear and nonlinear dependency of direct nitrous oxide emissions on fertilizer nitrogen input: A meta-analysis, *Agric. Ecosyst. Environ.*, *168*, 53–65.

Kurganova, I. N., and V. O. L. de Gerenyu (2010), Effect of the temperature and moisture on the N_2O emission from some arable soils, *Eurasian Soil Sci.*, *43*(8), 919–928.

Li, C. S. (2000), Modeling trace gas emissions from agricultural ecosystems, *Nutr. Cycling Agroecosyst.*, *58*(1–3), 259–276.
Liu, F. T., K. M. Ting, Y. Yu, and Z. H. Zhou (2008), Spectrum of variable-random trees, *J. Artif. Intell. Res.*, *32*, 355–384.
Liu, J. Y., et al. (2014), Spatiotemporal characteristics, patterns, and causes of land-use changes in China since the late 1980s, *J. Geogr. Sci.*, *24*(2), 195–210.
Liu, S. W., Y. M. Qin, J. W. Zou, and Q. H. Liu (2010), Effects of water regime during rice-growing season on annual direct N_2O emission in a paddy rice-winter wheat rotation system in southeast China, *Sci. Total Environ.*, *408*(4), 906–913.
Lu, Y. Y., Y. Huang, J. W. Zou, and X. H. Zheng (2006), An inventory of N_2O emissions from agriculture in China using precipitation-rectified emission factor and background emission, *Chemosphere*, *65*(11), 1915–1924.
McSwiney, C. P., and G. P. Robertson (2005), Nonlinear response of N_2O flux to incremental fertilizer addition in a continuous maize (Zea mays L.) cropping system, *Global Change Biol.*, *11*(10), 1712–1719.
Mei, B. L., X. H. Zheng, B. H. Xie, H. B. Dong, Z. S. Yao, C. Y. Liu, Z. X. Zhou, R. Wang, J. Deng, and J. G. Zhu (2011), Characteristics of multiple-year nitrous oxide emissions from conventional vegetable fields in southeastern China, *J. Geophys. Res.*, *116*, D12113, doi:10.1029/2010JD015059.
Novoa, R. S. A., and H. R. Tejeda (2006), Evaluation of the N_2O emissions from N in plant residues as affected by environmental and management factors, *Nutr. Cycling Agroecosyst.*, *75*(1–3), 29–46.
Parton, W. J., E. A. Holland, S. J. Del Grosso, M. D. Hartman, R. E. Martin, A. R. Mosier, D. S. Ojima, and D. S. Schimel (2001), Generalized model for NO_x and N_2O emissions from soils, *J. Geophys. Res.*, *106*(D15), 17,403–17,419, doi:10.1029/2001JD900101.
Perlman, J., R. J. Hijmans, and W. R. Horwath (2014), A metamodelling approach to estimate global N2O emissions from agricultural soils, *Global Ecol. Biogeogr.*, *23*(8), 912–924.
Roy, R., A. Finck, G. Blair, and H. Tandon (2006), Plant nutrition for food security A guide for integrated nutrient management. FAO Fertilizer and Plant Nutrition Bulletin, 16.
Saikawa, E., et al. (2014), Global and regional emissions estimates for N_2O, *Atmos. Chem. Phys.*, *14*(9), 4617–4641.
Schindlbacher, A., S. Zechmeister-Boltenstern, and K. Butterbach-Bahl (2004), Effects of soil moisture and temperature on NO, NO_2, and N_2O emissions from European forest soils, *J. Geophys. Res.*, *109*, D17302, doi:10.1029/2004JD004590.
Shcherbak, I., N. Millar, and G. P. Robertson (2014), Global metaanalysis of the nonlinear response of soil nitrous oxide (N_2O) emissions to fertilizer nitrogen, *Proc. Natl. Acad. Sci. U.S.A.*, *111*, 9199–9204.
Siebert, S., V. Henrich, K. Frenken, and J. Burke (2013), *Global Map of Irrigation Areas (v5)*. RFWU, Bonn, Germany and FAO, Rome, Italy.
Signor, D., C. E. P. Cerri, and R. Conant (2013), N_2O emissions due to nitrogen fertilizer applications in two regions of sugarcane cultivation in Brazil, *Environ. Res. Lett.*, *8*, 015013, doi:10.1088/1748-9326/8/1/015013.
Singurindy, O., M. Molodovskaya, B. K. Richards, and T. S. Steenhuis (2009), Nitrous oxide emission at low temperatures from manure-amended soils under corn (Zea mays L.), *Agric. Ecosyst. Environ.*, *132*(1–2), 74–81.
Skjøth, C. A., and C. Geels (2013), The effect of climate and climate change on ammonia emissions in Europe, *Atmos. Chem. Phys.*, *13*(1), 117–128.
Stehfest, E., and L. Bouwman (2006), N_2O and NO emission from agricultural fields and soils under natural vegetation: Summarizing available measurement data and modeling of global annual emissions, *Nutr. Cycling Agroecosyst.*, *74*(3), 207–228.
Tatti, E., C. Goyer, B. J. Zebarth, D. L. Burton, L. Giovannetti, and C. Viti (2013), Short-term effects of mineral and organic fertilizer on denitrifiers, nitrous oxide emissions and denitrification in long-term amended vineyard soils, *Soil Sci. Soc. Am. J.*, *77*(1), 113–122.
Troy, C., and J. Tang (2011), Effects of temperature and moisture stress on nitrous oxide production in agricultural soil, Semester in Environmental Science, Independent Project 2011.
Ussiri, D., and R. Lal (2012), *Soil Emission of Nitrous Oxide and Its Mitigation*, Springer, The Netherlands.
Van Drecht, G., A. F. Bouwman, J. M. Knoop, A. H. W. Beusen, and C. R. Meinardi (2003), Global modeling of the fate of nitrogen from point and nonpoint sources in soils, groundwater, and surface water, *Global Biogeochem. Cycles*, *17*(4), 1115, doi:10.1029/2003GB002060.
van Groenigen, J. W., G. J. Kasper, G. L. Velthof, A. van den Pol-van Dasselaar, and P. J. Kuikman (2004), Nitrous oxide emissions from silage maize fields under different mineral nitrogen fertilizer and slurry applications, *Plant Soil*, *263*(1–2), 101–111.
Wang, J. Y., Z. Q. Xiong, and X. Y. Yan (2011a), Fertilizer-induced emission factors and background emissions of N_2O from vegetable fields in China, *Atmos. Environ.*, *45*(38), 6923–6929.
Wang, J. Y., J. X. Jia, Z. Q. Xiong, M. A. K. Khalil, and G. X. Xing (2011b), Water regime-nitrogen fertilizer-straw incorporation interaction: Field study on nitrous oxide emissions from a rice agroecosystem in Nanjing, China, *Agric. Ecosyst. Environ.*, *141*(3–4), 437–446.
Xu, X. F., H. Q. Tian, G. S. Chen, M. L. Liu, W. Ren, C. Q. Lu, and C. Zhang (2012), Multifactor controls on terrestrial N_2O flux over North America from 1979 through 2010, *Biogeosciences*, *9*(4), 1351–1366.
Yang, J. F., X. R. Han, X. M. Zhan, and S. S. Sun (2007), Effects of different fertilization on N_2O emission in brown field (in Chinese), *Ecol. Environ.*, *16*(2), 560–563.
Yu, K. W., G. X. Chen, S. H. Yang, J. Wu, B. Huang, G. X. Huang, and H. Xu (1995), Role of several upland crops in N_2O emission from farmland and its response to environmental factors (in Chinese), *Chin. J. Appl. Ecol.*, *5*, 387–391.
Zhang, K. J., C. S. Jiang, Q. J. Hao, Q. W. Tang, B. H. Cheng, H. Li, and L. H. Cheng (2012), Effects of tillage-cropping systems on methane and nitrous oxide emissions from agro-ecosystems in a purple paddy soil (in Chinese), *Environ. Sci.*, *6*, 1979–1986.
Zheng, D. L., E. Raymond Hunt Jr., and S. W. Runing (1993), A daily soil temperature model based on air temperature and precipitation for continental applications, *Clim. Res.*, *2*, 183–191.
Zhou, F., et al. (2014), A new high-resolution N_2O emission inventory for China in 2008, *Environ. Sci. Technol.*, *48*(15), 8538–8547.
Zhou, M. H., B. Zhu, K. Butterbach-Bahl, X. H. Zheng, T. Wang, and Y. Q. Wang (2013), Nitrous oxide emissions and nitrate leaching from a rain-fed wheat-maize rotation in the Sichuan Basin, China, *Plant Soil*, *362*(1–2), 149–159.
Zhu, X., M. Burger, T. A. Doane, and W. R. Horwath (2013), Ammonia oxidation pathways and nitrifier denitrification are significant sources of N_2O and NO under low oxygen availability, *Proc. Natl. Acad. Sci. U.S.A.*, *110*(16), 6328–6333.
Zou, J. W., Y. Huang, Y. M. Qin, S. W. Liu, Q. R. Shen, G. X. Pan, Y. Y. Lu, and Q. H. Liu (2009), Changes in fertilizer-induced direct N_2O emissions from paddy fields during rice-growing season in China between 1950s and 1990s, *Global Change Biol.*, *15*(1), 229–242.